ICAS 2020 SHANGHAI
International Council of the Aeronautical Sciences
32nd Congress of the International Council of the Aeronautical Sciences
September 6-10, 2021
Pudong Shangri-La, Shanghai, China

CONCEPT OF A NEW SYSTEM SYNTHESIZING METEOROLOGICAL AND OROGRAPHIC INFLUENCES ON THE AIRPLANE SAFE ENERGY ENVELOPE

Xinying Liu[1,2], Leonardo Manfriani[2], Yongling Fu[1]

[1]Laboratory of Aerospace Servo Actuation and Transmission, Beihang University
[2]Centre for Aviation, School of Engineering, Zurich University of Applied Sciences

Abstract

An overproportioned number of accidents involving general aviation occur in complex terrain. According to the statistics included in the accident investigation reports published by the Swiss Transportation Safety Investigation Board (STSB), in some cases, pilots overestimated the energy reserves of their aircraft leading to a loss of control. In order to increase flight safety for private pilots in mountainous regions, on behalf of the Swiss Federal Office of Civil Aviation, the Centre for Aviation (ZAV) at the Zurich University of Applied Sciences (ZHAW) develops an energy management system for general aviation, which displays the remaining airplane's energy reserves taking into account meteorological information. As a result, the pilots can perform the necessary flight manoeuvres and adapt them to the situation so that the power envelope of the aircraft is not exceeded. The research project comprises two phases: i) concept and feasibility study and ii) prototype development. The phase one of the project has been recently completed. In this phase, the first implementation of the Energy Management system was carried out. To evaluate the system, a series of flight simulation tests were conducted in the ZAV's Research and Didactics Simulator (ReDSim). A group of experienced pilots participated in the pilot-in-the-loop simulations. This paper introduces the applied methodology on building the new flight simulation environment in the framework of the interdisciplinary research project. Further, the paper draws a summary of the concept study and gives an outlook of the prototype development in the next phase.

Keywords: energy management, aviation meteorology, general aviation, real-time flight simulation, atmospheric large-eddy simulation

1. Introduction

1.1 Motivation

An overproportioned number of accidents involving general aviation occur in complex terrain. According to the statistics included in the accident investigation reports published by the Swiss Transportation Safety Investigation Board (STSB), in some cases, pilots overestimated the energy reserves of their aircraft leading to a loss of control. In order to increase flight safety for private pilots in mountainous regions, on behalf of the Swiss Federal Office of Civil Aviation, the Centre for Aviation (ZAV) at the Zurich University of Applied Sciences develops an energy management system for general aviation, which displays the remaining airplane's energy reserves taking into account meteorological information. The paper presents a concept and feasibility study for the further development. In the first phase, it aims to find a simple and reliable display concept by means of suitable sensors which combine measured-/parameterized influences of meteorological parameters and the modelling of flight performance.

1.2 Literature review

In the past many works concerning atmospheric disturbance on flight safety were conducted. Japan Aerospace Exploration Agency (JAXA) was developing an onboard Doppler LIDAR [1][2] and a turbulence information system [3], which can detect wind shear, downbursts, wake-vortex, clear air turbulence and mountain wave in clear air condition. JAXA has installed the system on a small jet successfully flight-demonstrated its turbulence and windshear detection capability [4]. In addition, a developed novel airspeed advisory system shows lidar-predicted airspeed change for pilots' airspeed maintenance in turbulence or windshear conditions. In the framework of the European project Demonstration of Lidar based Clear Air Turbulence detection (DELICAT), a high-performance airborne UV Rayleigh lidar system was developed [6]. It aims at demonstrating a novel detection scheme for clear air turbulence (CTA). In commercial aviation, Clear Air Turbulence (CAT) encounter is a leading cause for injuries to cabin crew and passengers and causing M$ or M€ damage per year to airlines. Non-fatal aircraft accidents and incidents are concentrated en-route where in turn turbulence encounter is the main cause for such injuries [7].

Different from the above research works, the new Energy Management Envelope in General Aviation (EMEGA) system to be developed would be essentially installed in small general aviation (GA) planes and used by GA pilots during flying in the mountains. Due to that, convenient handling and low cost are the two highly weighted factors by selecting methods for the system development. Rather than turbulence detection, we focus on predicting vertical wind speed using geostatistical method.

Prior to the concept study, relevant accident reports published by STSB were studied. We considered accidents where a primary cause was an overestimation of the aircraft energy reserves by the pilots. This preliminary study is fundamental in the definitions of the project goals. The EMEGA system to be developed should be able to provide GA pilots with recommended take-off techniques considering engine power, take-off mass, runway length and meteorological information, e.g. temperature and wind fields. In airborne phase during a mountain flight, the local weather conditions and excess power are being kept updated.

1.3 Scope

The concept study of developing EMEGA system consists of the following five work packages:

- **Flight performance modelling:** This work package aims to create a general performance calculator that provides pilots with quantitative information of energy reserves, e.g. required take-off ground roll distance, rate of climb, energy required to perform a level turn etc. Initially, the PA-28-161's performance was modelled in calm air. By replacing the airplane specific databases (propulsion, geometry, and aerodynamics), the model can be adapted to other airplane models. In contrast to a real time flight simulation model, the full six degrees of freedom (DoF) equations of motion and dynamic responses of control elements are not considered in the flight performance calculator. The reverse engineering work used certified performance data in the Airplane Flight Manual (AFM) and the data in engine manual; and the propeller data provided by the propeller manufacturer.
- **Probabilistic extension of meteorological data in smaller scale:** Besides the flight performance calculator that developed in the previous work package, meteorological information has been integrated into the energy management system, which provides the pilot with vertical wind speed during mountain flight. The scope of this work package is to find a method to obtain vertical wind velocities with high spatial resolution (~100 m or less). Based on the literature review, Kriging and especially Cokriging were considered as promising methods to downscale vertical wind data with the help of good high-resolution terrain elevation available from Swisstopo (SwissAlti3D). The method of Co-Kriging was implemented in the first place. Unfortunately, due to the limited amount of time, a very rough simplification had to be made to avoid jeopardizing the other dependent work packages. In the first stage of the work, no clear correlation was found between terrain elevation data and vertical speed. Thus,

the Co-Kriging approach was stopped. It became clear that a meaningful downscaling of small-scale vertical wind variations (turbulence) with this approach is not doable for the atmospheric boundary layer. Further, a Kriging method was developed for downscaling vertical wind speeds. The resulting downscaled data is used for EMEGA graphic user interface (GUI).

- **Atmospheric turbulence modelling:** In order to generate highly resolved wind fields in the ReDSim well-established large-eddy simulation (LES) model, the Parallelized Large-Eddy Simulation (PALM) framework, was used in the concept study, focusing on a small mountainous region in Switzerland. For a more realistic representation of specific meteorological situations, PALM was driven with boundary conditions extracted from the COSMO-1 reanalysis of MeteoSwiss. The environment model in the ReDSim was modified to include a new subsystem simulating atmospheric disturbance. The essential variables (wind components, temperature, and pressure) were extracted from the PALM output and fed into the subsystem after interpolation to obtain the values at any instant and any aircraft position. Within the subsystem, it is also possible to generate statistical atmospheric turbulence based on the Dryden turbulence model which refers to the military specification MIL-F-8785 [8].
- **Concept of information processing:** As an information processing tool, the EMEGA GUI was developed in the framework of this work package. The GUI includes a generic flight performance calculator that can supply the pilot with quantitative information of energy reserves as described in the previous section. The first version of EMGEA GUI in the framework of this simulation includes the certified performance data and geometry database in the AFM of Piper PA-28-161 Warrior II, and a pre-processed meteorological database.
- **Components assembly in the ReDSim and flight simulation test:** To evaluate the first implementation of EMEGA system, an appropriate flight simulation environment was built in the ReDSim. Figure 1 gives an overview of the flight simulation environment, which consists basically of two modules, flight simulation model and EMEGA GUI. The two modules are running at the different hosts in the same network. The sensor data from flight simulation model are transferred to EMEGA GUI via User Datagram Protocol (UDP). In the first step, the existing PA-28 flight simulation model in ReDSim developed in [9] were modified. Several modifications on propulsion model and aerodynamics database were carried out. Further, the environment model and aircraft equations of motion (EoM) were modified to include the new subsystem simulating atmospheric disturbance. The first implementation was tested using pilot-in-the-loop flight simulations. A group of test pilots were invited to the ReDsim. The test campaign aims to prove the feasibility of the concept and to collect subjective feedback from the experienced pilots for the further prototype development.

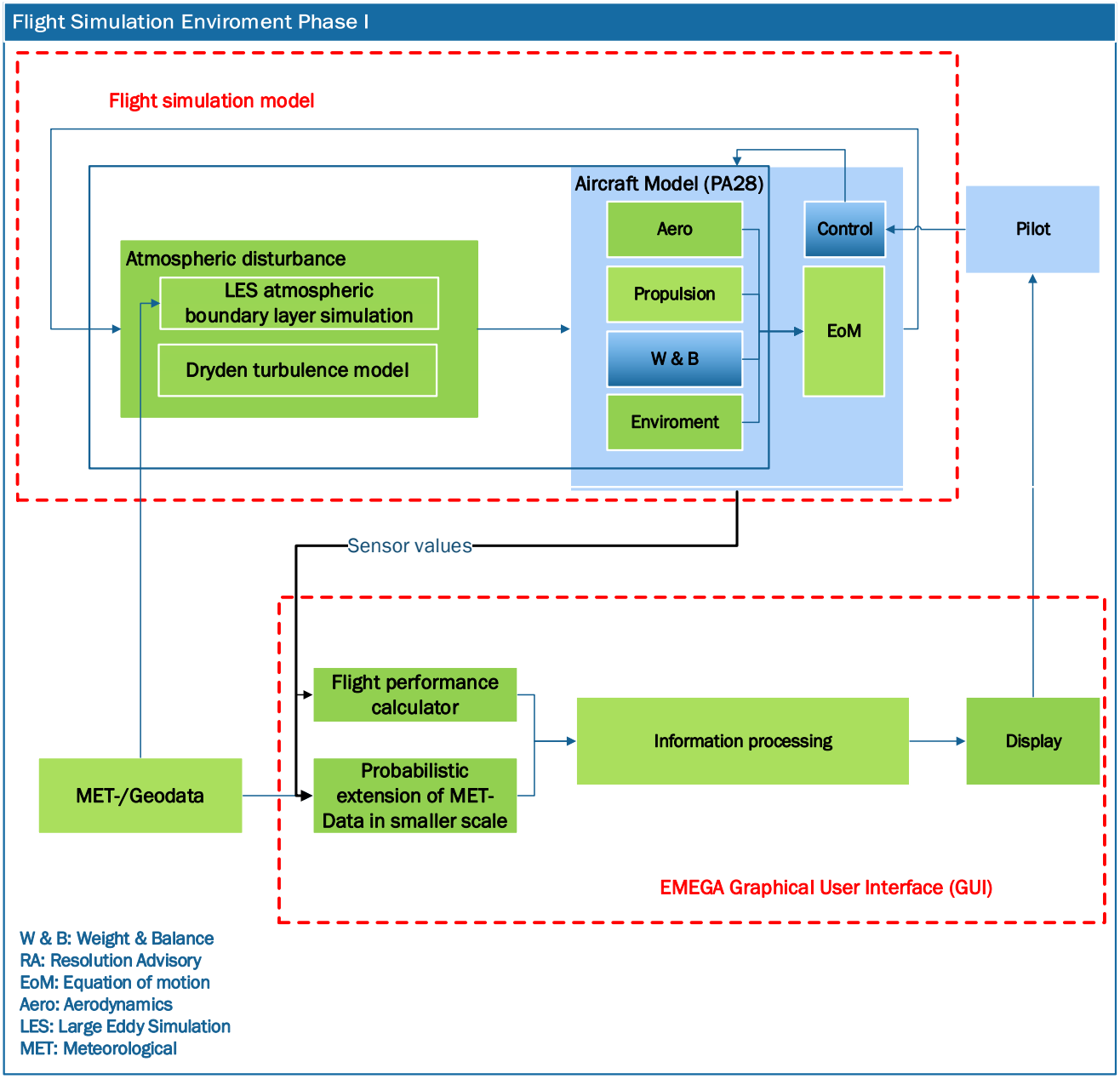

Figure 1 – Overview of flight simulation environment

2. Data and Methods

2.1 Data used for flight performance modelling

The work of flight performance modelling follows a reverse engineering approach. The engine model of the developed flight performance calculator is built based on the data [10] published by the engine manufacture Lycoming. As a reference, the certified data of engine in-flight performance in the AFM [11] were reconstructed and integrated in the flight performance calculator.

- **Engine data [10]**: O-320-B and D Series (Except O-320-B2D, -B2E, -D2J)
  a. Sea level and altitude performance, maximum power mixture (curve N0. 11260-A)
  b. Sea level power curve (propeller load horsepower curve), full rich (curve No. 11259)
  c. Engine Power and Specific Fuel Consumption at Constant Engine RPM and Manifold Pressure (Figure 3-1)
- **Propeller data:** 74DM6-0-60, fixed pitch angle
  a. Advance ratio J vs. thrust coefficient c_t
  b. Advance ratio J vs. power coefficient c_p

c. Advance ratio J vs. propeller efficiency η

- **Reference data [11] :**
  a. Section 5, performance chart, figure 5-15, Engine Performance Best Power Mixture
  b. Section 5, performance chart, figure 5-23, Best Power Cruise Performance

2.2 Benchmarking meteorological data

In order to validate the 2D-data generated from the co-kriging and kriging procedures as well as from the computational fluid dynamic large eddy simulations (LES), measured data of horizontal wind components as well as temperature and humidity are required. Due to the easy topographic conditions and accessibility, the Swiss midlands are by far better covered with automatic measurement stations for meteorological data than the Alpine region. For instance, the SwissMetNet [12] weather station network counts over 150 stations reporting wind direction and speed. From those, a little bit more than 30 stations are installed at an altitude higher than 1500 meters above mean sea level.

For the selected area of study, four SwissMetNet stations were available for benchmarking purposes. However, only one station (COV/Piz Corvatsch) was located on a mountain ridge at an altitude of 3311 m as a satisfactory station representing best the state of the undisturbed free atmosphere. The other stations (BEH/Passo del Bernina/2271m, SIA/Segl-Maria/1806m, SAM/Samedan/1711m) were unsuitable for free-flow benchmarking. The data of COV was obtained via the IDAweb interface, which grants research institutions a free access to surface meteorological measurement data from the SwissMetNet and other networks. The data of COV was obtained via the IDAweb interface, which grants research institutions a free access to surface meteorological measurement data from the SwissMetNet and other networks.

As a complement to the SwissMetNet data, IMIS data were taken from three further stations for benchmarking purposes: Station BER1 (Lagalb/2956m), BEV1 (Cho d'Valetta/2490m) and LAG2 (Lagrev/3085 m). As for the SwissMetNet data, the meteorological data from the IMIS (Interkantonale Mess- und Informationssystem) stations could be downloaded directly from the data portal IDAweb provided by MeteoSwiss and used for further analysis.

2.3 COSMO-1 data

The LES model PALM requires 3D boundary conditions for the essential variables (U & V wind speeds, temperature, pressure and specific humidity). Those can be set either as fixed fields along the model boundary, or as time-varying fields. In transitioning simulations, a specific situation needs to be reanalyzed, time-varying fields need to be used. For PALM, a routine ("INIFOR") has been developed which automatically reads and converts 3D fields from the regional weather model "COSMO" to the final format required for the LES. The Consortium for Small-scale Modeling (COSMO) is a collaborative group of eight hydro-meteorological offices whose main aim was to develop a regional model. The non-hydrostatic model "COSMO" was born, and is used operationally all around the globe, however with a strong focus on Germany and Switzerland. There, the COSMO model is running in different resolutions, where the highest resolution currently used is of 1.1 km (COSMO1: ~1.11 km N-S and ~0.75 km E-W) and spreads over 80 terrain following coordinate levels (following the smooth level vertical scheme, SLEVE). Next to the 5 variables listed above, the height of the half-model level (HHL) as well as the soil type, soil temperature and soil moisture were also ordered in order to approach the simulation as close as possible to the reality.

It is important to note that even a highly resolved topographic resolution like the one of COSMO-1 is still rather limited when performing studies in complex terrain like the Alpine region. Depending how the domain of the LES is localized, different boundary conditions from COSMO-1 will be fed into the PALM model, depending through which grid cells the PALM boundaries will be defined. As the topographic resolution of COSMO1 is much coarser than the one in PALM, the horizontal wind fields may differ significantly from each other. Although this problem will mainly concern the lowermost model layers, this may generate unwanted artefacts in the LES results. Therefore, a visual selection of the COSMO-1 winds was performed in order to set the PALM domain as well as possible.

Besides COSMO-1 data were downscaled by using geostatistical methods as well.

2.4 Methods

This section includes the applied methods in the framework of the concept study. Following, first the flight performance model is descripted. The second and third part explain the geostatistical methods for downscaling meteorological data. Then, the LES model including boundary conditions are briefly described. The last part gives a summary of the implementations of EMEGA GUI and modifications on flight simulation model.

2.4.1 Flight performance modelling

This part shows the concept of ZHAW Flight Performance Calculator (ZFPC) for estimating flight performance of propeller aircraft with fixed pitch angle. The work included here is a reverse engineering work based on AFM data and the data in the engine manual. An engineering method has been applied primarily to provide the pilot with airplane performance data during flight. The left illustration in Figure 2. The calculator consists of three main submodules:

- **Loads calculation:** propulsion trust, aerodynamic and airfield forces are calculated. Further, the submodule includes a block named Meteorology, which calculates loads from the environment. To calculate propulsion trust, the provided engine performance data needs to be tuned. The flowchart on the right-hand side in Figure 2 shows the general approach predicting shaft horsepower (SHP) and the corresponding propeller speed. The function engine tuning will be explicitly discussed in this paper.
- **Performance calculation:** Based on Engineering Sciences Data Unit (ESDU), kinematic equations were implemented to predicts the performance in five phases separately: take-off, landing, climb, descent, and cruise.
- **General:** The calculator provides several functions for tuning purpose. It is planned to extend the model to predict performance of other airplanes in the future. With the tuning module, the calculator can generate aerodynamic and engine database for another airplane based on the performance data in its AFM. The AFM data in [11] was digitized and included in the current database.

Engine tuning

In general, engine and propeller manufactures provide airplane manufactures with dedicated engine and propeller deck data, including shaft horsepower, exhaust trust and fuel consumption, in order to establish AFM charts for the purpose of airplane certification. The conducted work in this part followed a reverse approach. The certified data in the AFM and the published data in the engine manual were used for database tuning in pre-processing. The obtained database is used for predicting airplane performance.

In the first line, engine data included in the engine manual needs to be tuned, as the data convers wide variations of engine speed-power characteristics, even for engines of similar power output. The tuning procedure starts from the propeller load horsepower curve (refer to engine data a in section 2.1), which defines the maximum available shaft horsepower at each value of RPM. The curve from the manufacturer shows the average values of different propellers installed on the engine. It gives a generic view of the engine performance. The main task of engine tuning is to obtain an appropriate correlation coefficient k between SHP and RPM (see eq.1) K depends on mixture setting and flight condition.

$$SHP = k(mixture, flight\ condition) \cdot RPM^3 \tag{1}$$

In the following, tuning procedures for cruise power and climb power are described. For the best cruise power (BECP) mixture, the tuning procedure is straightforward, since the engine in-flight performance data (see reference data a in section 2.1) is included in the AFM. The equation (1) becomes

$$SHP_{AFM} = k_{lycoming} \cdot k_{BECP}(t, h, c) \cdot {RPM_{AFM}}^3 \tag{2}$$

where:

h flight altitude in [m], *t*: temperature [K], *c* percentage of rated power [-], *RPM*: engine speed in [RPM], *BECP* denotes best cruise power mixture, *AFM* denotes value derived from AFM and

Lycoming denotes value derived from engine manual.

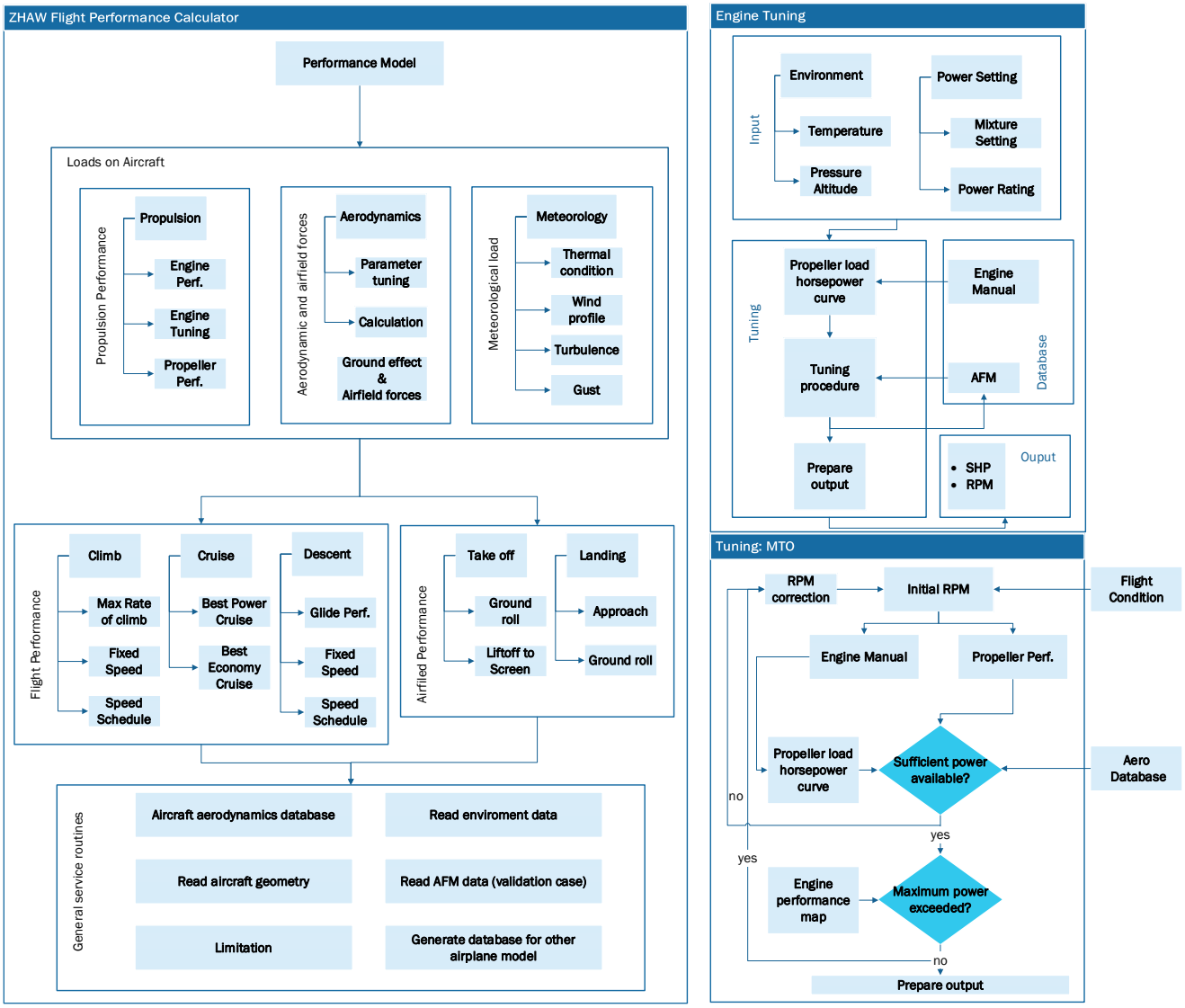

Figure 2 – Overview of fight performance calculator

Following equation (2) 3D look-up table of k_{BECP} *(t,p,c)* for best cruise power mixture was developed. By giving an RPM, the SHP can be estimated. The estimated SHP in tuning mode is considered as the maximal available power in the specified condition. For the power setting Maximal Cruise Power (MCP) with full throttle, the 3D look-up table is not valid anymore, since the percentage of rated power with full throttle is not specified in the AFM chart. In addition, it cannot be assumed either that the rated power can be reached at all flight conditions. The maximal available cruise power is to be calculated by using the maximal cruise speed V_{BECP} defined in the AFM data (see reference data b in section 2.1), which is mathematically described as follows

$$SHP_{MCP} = SHP_{BCP}[V_{BCP}(t,h)] \cdot k_{full\_throttle} \tag{3}$$

where:

$k_{full\_throttle}$ tuning factor for full throttle setting, *BCP* denotes full throttle with best cruise power.

Based on the results of (2) and (3), the SHP with economy cruise mixture can be calculated by including a tuning factor $k_{full\_throttle}$ as follows

$$SHP_{BECP} = SHP_{BCP} \cdot k_{lean\_mixture} \tag{4}$$

During the climb phase the mixture setting is full rich. The shaft horsepower with full throttle can be defined as:

$$SHP_{full\_rich} = SHP_{MCP} \cdot k_{full\_rich} \quad (5)$$

where:

k_{full_rich} tuning factor for full rich mixture (refer to reference data c in section 2.1).

As take-off is highly dynamic manoeuvre, the iterative tuning procedure for Maximal Take-Off (MTO) power illustrated in Figure 2 is a separated module, which is integrated in take-off performance calculation directly.

2.4.2 Kriging

Kriging is a geostatistical interpolation method based on autocorrelation. This interpolation method is to estimate a value $z^*(u_0)$ (the asterisk represents the estimation) at a location u_0 in a spatial construct. This value could be any parameter (here called z) which is accompanied by the information of the location where it was measured. In the EMEGA system, the parameter will be the vertical wind speed w. For each measured value w, the coordinates (lat, lon) as well as the altitude (h) are given. The estimate $z^*(u_0)$ is based on the known values $z(u_i)$ from other locations in this construct.

The process for an estimation at any point in the given data grid is the following:

i. The variogram for three orthogonal axes is calculated. Each variogram provides a range which describes how far the autocorrelation in this axis reaches. The three ranges together give a full 3D model of continuity. The formula used to calculate one point in a variogram is the following:

$$\gamma(h) = \frac{1}{2N(h)} \sum_{\alpha=1}^{N(h)} [z(u_\alpha) - z(u_\alpha + h)]^2 \quad (6)$$

With h as the lag length (for example the number of observations in between two data points), γ(h) as the variogram value for the given lag length, $N(h)$ as the number of data point pairs given the lag length, $z(u_a)$ as a data point and $z(u_a+h)$ as a data point with one lag length distance from $z(u_a)$.

ii. Calculate the distance matrix, a matrix containing a scaling factor which expresses the distance between two data points. The scaling factor has meaningful values between 0 and 1. The following equation is used to calculate a scaling factor h_s:

$$h_s = \sqrt{\left(\frac{h_{maj}}{a_{maj}}\right)^2 + \left(\frac{h_{min}}{a_{min}}\right)^2 + \left(\frac{h_{vert}}{a_{vert}}\right)^2} \quad (7)$$

With $a_{()}$ as the range from the variograms in the respective direction and $h_{()}$ as the lag distance in the respective axis direction. The axes are described as major (maj), minor (min) and vertical (vert) axis.

iii. Based on the three variograms, a nested variogram can be calculated with the following formula:

$$\gamma(h_s) = C_1\gamma_1(a_1h_s, a_1) + C_2\gamma_2(a_2h_s, a_2) + C_3\gamma_3(a_3h_s, a_3) \quad (8)$$

where h_s is the scaling factor from the distance matrix, $\gamma(h_s)$ is the variogram value for the nested variogram for the respective scaling factor, $\gamma_i(a_ih_s, a_i)$ is the value for a variogram in one of the main directions with the range a_i and at lag length a_ih_s, and C_i as the sill value of the respective variogram.

iv. With the nested variogram and the distance matrix, a variogram matrix can be calculated, containing the nested variogram value between any two meteorological data points.

v. Based on the variogram matrix the covariance matrix can be obtained, containing the covariance between any two meteorological data points.

vi. The covariance vector containing the covariance between every data point and the location u_0 is calculated.

vii. The residual for each data point has then to be calculated, giving the residual vector.

viii. With the covariance matrix and the covariance vector, the weight vector can be calculated.

ix. Finally, using the weight vector and the residual vector, the estimation $z^*(u_0)$ can be calculated.

2.4.3 Co-Kriging

Co-Kriging is a generalization of Kriging in that it uses not only the spatial correlation of the variables(s) of interest but also the intervariable spatial correlation, and allows estimation of the variable(s) at an unsampled location using not only data for variable but also data from the correlated variables [13]. The estimation $z^*(u_0)$ in the previous section with Kriging can also be influenced by other parameters (e.g. *p* and *q*), which are known at other locations $(p(u_i), q(u_i))$ as well as at the location u_0 $(p(u_0), q(u_0))$. Hence, the estimation of $z^*(u_0)$ with a poorly sampled variable z can be improved by a well-sampled variable *p* or *q*. In the case discussed in this paper, the poorly sampled variable would be the vertical wind speed and the well-sampled variable would be the slope of the terrain in wind direction.

To perform Co-Kriging, cross variogram needs to be determined. As the considered two variables in this study have significantly different spatial resolution, a pseudo-cross-variogram introduced in [14] was implemented for the calculation. This estimation does not require that the sample data of the considered variables are at the same location.

For Co-Kriging, a well-sampled variable with a good correlation is needed. In this study the target value of the correlation between vertical wind speed and the slope of the terrain in wind direction was set to 0.6. In general, with high atmospheric stability, regular terrain-following lee-waves are known to form in approximate direction of the mean atmospheric flow. Several parameters, Brunt-Väisälä frequency *N*, Scorer parameter *l* and Froude number *Fr* were used as stability indicators. The Brunt-Vaisala frequency, also called buoyancy frequency, is the frequency of the vertical displacement of a parcel of air in statistically stable atmosphere, which is defined as follows

$$N = \sqrt{\frac{g}{\theta}\frac{d\theta}{dz}} \tag{9}$$

with: ϑ *[K]* potential temperature and *z [m]* altitude, and gravitational acceleration *g* $[m/s^2]$.

The Scorer parameter is used to describe whether waves will develop or not. It combines the Brunt-Väisälä frequency *N* with characteristics of the vertical wind profile. If *N >1,* the lee waves are not negligible, the Scorer parameter is given by

$$l^2(z) = \frac{N^2}{U^2} - \frac{\left(\partial^2 U/\partial z^2\right)}{U} \tag{10}$$

with: *U (z)* the vertical profile of the horizontal wind.

High Scorer values correspond to a high stability while smaller values correspond to a lower stability.

If l2(z) strongly changes with altitude it is a good condition for trapped lee waves. Propagating mountain waves are more likely if l2(z) is not changing with height. Lastly, when l2(z) is increasing with height, the development of gravity waves is not favoured.

The dimensionless Froude number (*Fr*) gives the ratio of inertial and gravitational forces of a flow by

$$Fr = \frac{u_0}{\sqrt{gL}} \tag{11}$$

with: u_0 horizontal windspeed *[m/s]* and *L* characteristic length *[m]* (distance to ground in this case).

2.4.4 Atmospheric turbulence modelling

In order to generate highly resolved wind fields, the Parallelized Large-Eddy Simulation Model (PALM) was used. PALM is open source code. The model system has been mainly developed by the PALM group at the Institute of Meteorology and Climatology of Leibniz Universität Hannover, Germany. Originally, PALM was based on non-parallelized LES code described in [15]. During the last years, since the version 4.0 [16], PALM has been significantly improved. The paper of Maronga et al. ([17]) includes the latest changes in PALM 6.0. The code is becoming increasingly popular in atmospheric research and ocean flow simulation. Several national (German) and international research groups have participated in code development. Since 2019 the Centre for Aviation has been using the simulation model to simulate atmospheric flow conditions for different customers in Switzerland [18].

The PALM model is a pressure-based and finite-difference solver, which solves non-hydrostatic,

filtered, incompressible Navier–Stokes equations. By default, PALM estimates six fundamental quantities: three velocity components on a Cartesian grid, potential temperature, and water vapor mixing ratio. This section gives a brief introduction of the model comprising the following four aspects:

Governing equations

The model solves incompressible equations in Boussinesq-approximated form, filtered based on a spatial scale separation approach described in [19], or an anelastic approximation. For Boussinesq approximation, a predictor corrector method [20] is used to predict the modified perturbation pressure after every time step. In general, PALM solves the Poisson equation using direct Fast Fourier Transform (FFT) in case of cyclic lateral boundary conditions. Several FFT methods have been implemented (for details refer to the PALM introduction [16]). For anelastic approximation, the flow is treated as incompressible, allowing for density variations with height, while variations in time are not permitted [16].

Turbulence closures

PALM has two modes dealing with turbulence closures: i) the LES mode; ii) the Reynolds-averaged Navier-Stokes Simulation (RANS) mode. In the default LES mode, PALM uses a Sub-grid scales (SGS) model for the modelling of unresolved scales. The SGS model is a 1.5-order closure according to Deardorff's theory [21][22][23]. In general, it assumes that the SGS energy dynamic is proportional to the local gradients of mean quantities. Besides, a dynamic SGS following the Moktharpoor & Heinz ([24]) has been implemented recently in the new version. PALM's RANS mode offers two standard turbulence models to parameterize turbulence kinetic energy (k): *k-l* (mixing length) model according to and *k-ε* (dissipation rate of k) according to [26][27]. In the first stage of simulation work, the RANS model was to obtain key quantities for the EMEGA system, e.g. wind components. It aims to consider mesoscale processes. The advantage is that RANS mode requires less time costs. Whin the domain of interest with fine nested grid, the LES model was enabled for some further detailed spectral analysis.

Discretization

PALM's grid configuration is following the Arakawa staggered C-grid (Harlow) [19] for the spatial discretization. The calculation domain discretized using finite differences and equidistant horizontal grid spacings. An upwind-biased 5th-order (refer to [28]) is used for the discretization of advection terms in the governing equations, in combination with a 3rd-oder Runge-Kutta scheme described in [29].

Boundary conditions

In general, PALM provides a variety of boundary conditions, e.g. Dirichlet and Neumann boundary conditions. While PALM can be run with non-cyclic horizontal boundary conditions described in [30][31]. In this study, PALM was configured to allow large-scale forcing of meteorological fields from the COSMO model onto its lateral domain boundaries. The region Samedan in Switzerland, 133'915 – 152'347 latitude and 774'572 – 799'148 longitude (in CH1903+ coordinates) was chosen as calculation domain.

For the topography, original 30-meter Shuttle Radar Topography Mission (SRTM) elevation data were downloaded using an open source platform Quantum Geographic Information System (QGIS). This data was further downscaled in 5 m and then used for generating PALM input file. The PALM results are exported in NetCDF-4 (Network Common Data Form, version 4.0) format.

2.5 Concept of information processing

As a demo version of the EMEGA system, a GUI was developed using App Designer in the software MATLAB and integrated in the cockpit of the ReDSim (see Figure 3). The work of flight performance modelling aims to perform energy reserves combining a risk map that predicts vertical wind speed. The risk map is shown in a separated panel and it is been kept updating during flight.

The EMEGA GUI contains seven modules: 1) main menu, 2) weight and balance, 3) take-off performance, 4) cruise performance, 5) climb performance, 6) excess power for level turn and 7) risk map. Several functions of flight performance calculator were modified and integrated in the EMEGA GUI that provides pilot with quantitative information of energy reserves, e.g. required take-off ground roll distance, rate of climb and energy required to perform a level turn. Besides, it includes a pre-

processed meteorological database. The data of COSMO-1 reanalysis were downscaled using kriging method. The instrument displays zones of potentially dangerous regions with high vertical wind speed, using the downscaled data. The categories of the display are defined in Table 1.

Figure 4 shows an example of module 7 risk map combined excess power for level turn displayed in the main panel. The categories are shown as coloured areas. They were calculated using the values of all data layers available within +/- 500 m height of the current flight altitude. The category at a certain position (certain coordinates) is defined by the highest category found in all layers. Furthermore, the contours of Cat 3 zones of data layers outside of the +/- 500 m are displayed in red. In fact, the layers considered for these contours are between -500 and -1000 meters and +500 to +1000 meters of the current flight altitude. All chosen heights mentioned here can be changed and adjusted if necessary. In addition, the flight position and the recent flight path are plotted (red triangle and blue path).

Figure 3 – EMEGA GUI integrated in the cockpit of the ReDSim

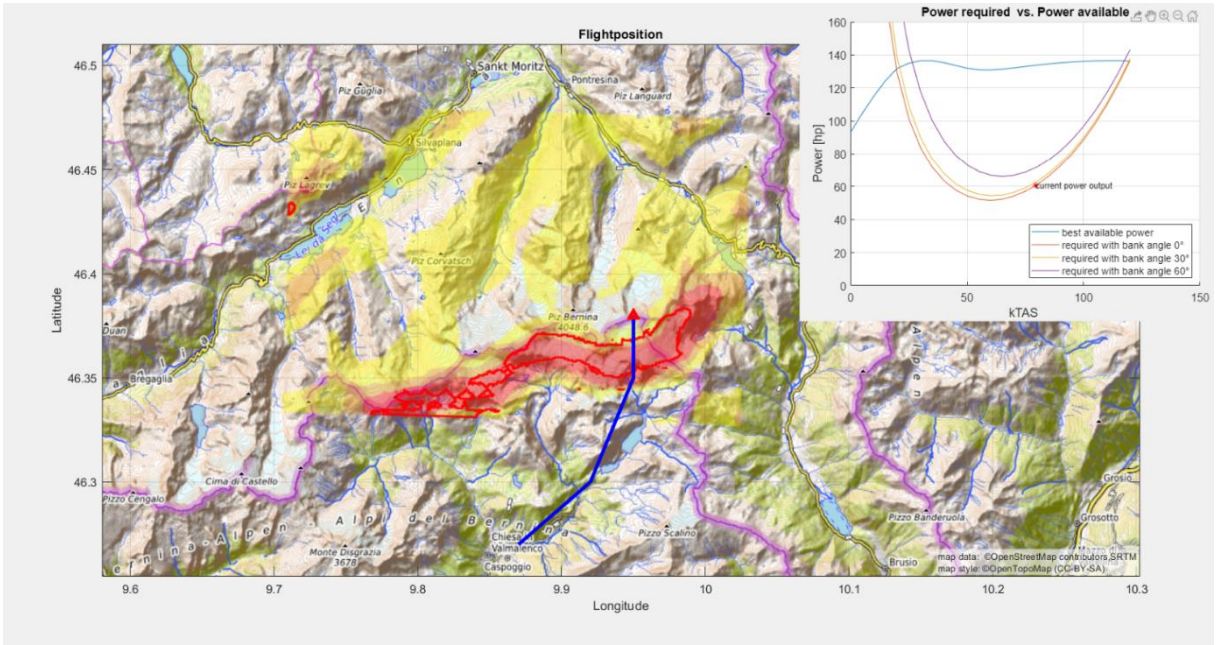

Figure 4 – Risk map and excess power for level turn

Table 1 – Vertical wind categorization

Category	Range of vertical wind in m/s	Colour in display
Cat 0	>= 0	No colour
Cat 1	0 < x < (-1)	Yellow
Cat 2	(-1) < x < (-2)	Orange
Cat 3	<= (-2)	Red

2.6 Flight simulation environment

- **Modifications of propulsion model**: In the project literature review [32], it was pointed out that the current engine model of PA-28 flight simulation model would need to be further improved:
  - Flight performance data generated by the simulation model were significantly lower than the certified data in the AFM [11]. This is considered as insufficient for the purpose of proofing the flight simulation model's validity.
  - Several factors limited model accuracy: the effect of mixture settings was neglected; propeller load horsepower curve was valid only for full rich mixture and sea level standard conditions; the generic, performance-oriented treatment of engine dynamics and propeller-engine matching did not allow reliable prediction of quantities such as take-off distance and maximum cruise speed.

  Such issues were addressed in the framework of this work package and a new propulsion model was developed, having the following characteristics:

  - The generic piston engine model now calculates engine output as a function of bot throttle lever position and mixture setting.
  - Quantities such as manifold pressure and brake horsepower are computed by fitting data from engine performance charts.
  - Propeller thrust, torque and absorbed power are calculated based on the characteristic curves provided by the propeller manufacturer.
  - The dynamics of the engine and the matching of engine and propeller are modelled considering the inertial of the propeller in the torque equilibrium
  - The correlation between engine power setting and steady-state RPM has been obtained through mapping of flight test data in the framework of [9][33]
- Modification of aerodynamics database: In the previous version of the PA-28 model, drag coefficients had been tuned to obtain realistic performance with the current version of the propulsion model. Following the upgrade of the propulsion model, a new estimation of the aircraft drag polar curve (in terms of zero-lift drag coefficient and Oswald factor) was carried out, based on the comparison of flight simulation test output against the cruise and climb performance data reported in the AFM [11].
- **Modifications of propulsion model**: The environment model and aircraft equations of motion have been modified to include a new subsystem simulating atmospheric disturbance. The latter can be generated in two ways:
  - By importing data from atmospheric boundary layer simulations obtained using PALM. The PALM output data are converted from the netCDF format and interpolated to obtain the values of pressure, temperature, wind velocity components and angular rates, at any instant and any aircraft position within the test area, where PALM data is available
  - By generating statistical atmospheric turbulence based on the Dryden model of power spectral density introduced in [8]. The Dryden model can be activated either anywhere throughout the simulation or only when the aircraft is outside the PALM domain
- **Integration of the EMEGA GUI into the ReDSim environment:** The flight simulation model and EMEGA GUI are running on two different computers but in the same network. The sensor data from flight simulation model are transferred via User Datagram Protocol (UDP)

3. Results and discussion

3.1 Flight performance modelling

This section presents the validation results obtained in three phases: take-off, climb and cruise, which are considered as critical in this project. The present performance assessment follows an Estimated versus AFM (EvA) approach. The common flight test conditions published in AFM were directly replicated in the performance calculator.

3.1.1 Take-off performance

The results of take-off performance are summarized in Figure 5. In general, the estimated data shows good agreement with AFM data. The average deviations lie within ±4% of ground distance and total landing distance. The standard deviation is less than 4%. This is considered acceptable for the purpose of demonstrating the model's validity. It can be concluded that the take-off performance can be predicted by the calculator with acceptable precision.

3.1.2 Climb performance

The estimated values of Rate of Climb (RoC) and the corresponding conditions are directly plotted in the AFM chart [11], section 5, Figures 5 - 17 . The estimated data has a good agreement with the AFM data. The average deviations lie within ±4% of the RoC. The standard deviation is 2.6%. It can be concluded that the climb performance can be predicted by the calculator with acceptable precision.

3.1.3 Cruise performance

Table 2 compares engine and cruise performance of the data AFM [11] with the estimated data. As described in the previous section, the RPM defined in the AFM in section 5, Figures 5 -15 were kept as input for performance calculation in engine tuning mode of the calculator. The estimated engine power has slightly lower values than AFM data. The average deviations lie within ±4% of SHP. The standard deviation is 1.0%. Further, the cruise speeds were calculated and compared with the AFM data (see Figure 6). The standard deviation of cruise speed is 1.4%. In general, it can be concluded that the engine and cruise performance can be predicted by the calculator with acceptable precision. In order to obtain more accurate cruise performance at high altitude and temperature, it is necessary to conduct flight tests to improve the current engine database.

3.1.4 Conclusion

Based on the AFM of the PA-28-161 Warriors II aircraft, propeller performance data of the 74DM6-0-60 engine provided by Sensenich and the Lycoming O-320-B and D series engine data in the manual, a performance calculator was developed. The estimated performance data was compared with AFM data. The results show a good agreement and demonstrate that the aircraft's performance can be predicted with acceptable precision.

3.2 Meteorological parametrization

3.2.1 Co-Kriging

The first step of Co-Kriging is to calculate the slope of the terrain in wind direction $\frac{\partial D}{\partial w}$ which is defined as follows

$$\frac{\partial D}{\partial w} = \frac{\partial D}{\partial x}\sin\varphi + \frac{\partial D}{\partial y}\cos\varphi \tag{12}$$

with wind direction φ and the slopes of the terrain in cartesian coordinate system $\frac{\partial D}{\partial x}$ and $\frac{\partial D}{\partial y}$.

COSMO data on 11.09.2019 at 09:00 UTC were used for the Co-Kriging calculation. The area around Thunersee, Briezersee and Sanerraatal (in CH1903+ coordinates: 606'578 – 687'706 in x direction and 150'865) was taken into account. In general, the COSMO model uses a terrain following vertical coordinate. The vertical grid is specified as a three-dimensional field. The 3D field is the height of the half-model levels (HHL), so-called SLEVE2 layers. Figure 7 (left) shows the quantity mean height above ground of all SLEVE layers of the COSMO data. The maximal altitude of interest in this study is about 4000 m, the SLEVE2 layers with a mean height above ground less than 4000 m were used for the further calculation. HHL values of the SLEVE2 layers to be evaluated are plotted in longitudinal direction in Figure 7 (right).

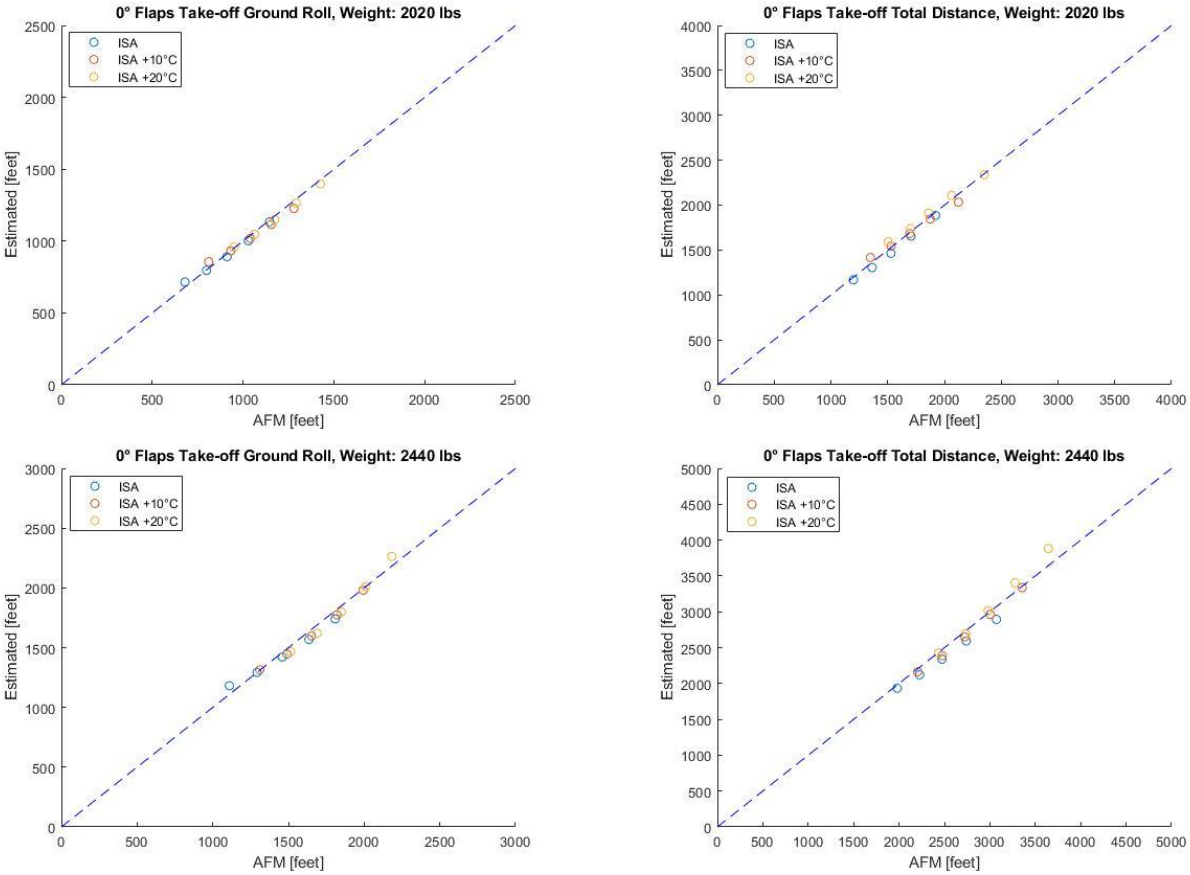

Figure 5 – Take-off performance: estimated data vs AFM data

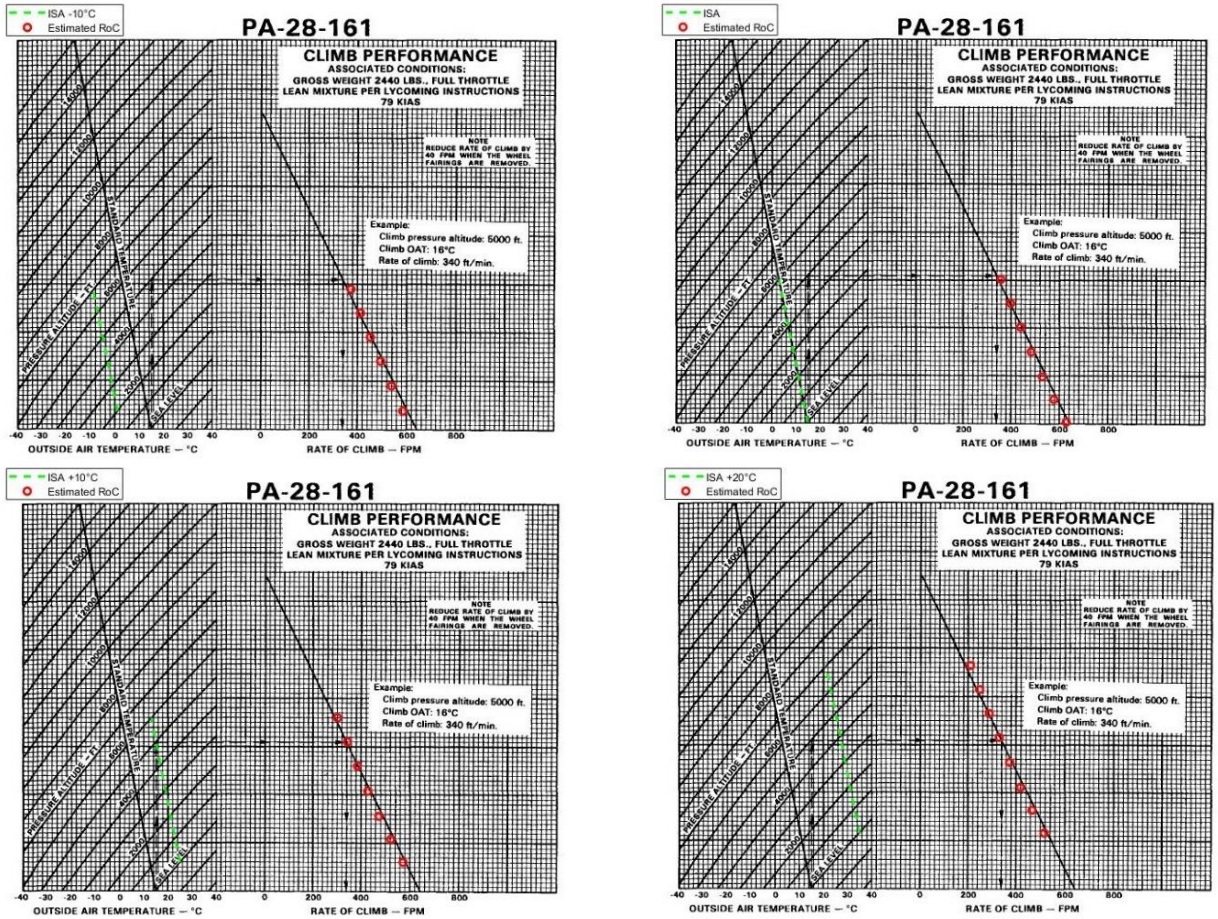

Figure 6 – Take-off performance: estimated data vs AFM data

Table 2 – Cruise performance: estimated data vs AFM data

PA 28-161	Test Condition			Power Setting		AFM		Estimated		EvA	
Test Point	Press. Altitude	Mass	ISA	SHP	Mixture	SHP	Air-Speed	SHP	Air-Speed	Δ RPM E.-A.	Δ kTAS E.-A.
[#]	[ft]	[lbs]	[°C]	[%]	[-]	[HP]	[kTAS]	[HP]	[kTAS]	[-]	[-]
1	2000	2300	-20	55	BCPL	88	95.1	84.7	92.7	-3.7%	-2.5%
2	4000	2300	-20	55	BCPL	88	97.0	85.5	94.4	-2.8%	-2.7%
3	6000	2300	-20	55	BCPL	88	98.9	85.8	95.9	-2.5%	-3.0%
4	2000	2300	0	55	BCPL	88	97.4	85.7	94.7	-2.6%	-2.8%
5	4000	2300	0	55	BCPL	88	99.4	86.5	96.4	-1.7%	-3.0%
6	6000	2300	0	55	BCPL	88	101.3	86.7	97.7	-1.5%	-3.6%
7	2000	2300	20	55	BCPL	88	99.6	87.1	96.7	-1.1%	-2.9%
8	4000	2300	20	55	BCPL	88	101.6	87.7	98.2	-0.4%	-3.3%
9	6000	2300	20	55	BCPL	88	103.5	87.8	99.3	-0.3%	-4.1%
10	2000	2300	-20	65	BCPL	104	104.5	100.1	100.3	-3.7%	-4.0%
11	4000	2300	-20	65	BCPM	104	106.6	100.4	102.1	-3.5%	-4.2%
12	6000	2300	-20	65	BCPM	104	108.6	100.1	103.6	-3.8%	-4.6%
13	2000	2300	0	65	BCPM	104	107.0	100.3	102.5	-3.5%	-4.2%
14	4000	2300	0	65	BCPM	104	109.1	100.5	104.2	-3.3%	-4.5%
15	6000	2300	0	65	BCPM	104	111.1	100.1	105.6	-3.7%	-5.0%
16	2000	2300	20	65	BCPM	104	109.3	101.0	104.5	-2.9%	-4.3%
17	4000	2300	20	65	BCPM	104	111.4	101.1	106.1	-2.8%	-4.8%
18	6000	2300	20	65	BCPM	104	113.4	100.5	107.3	-3.3%	-5.4%
19	2000	2300	-20	75	BCPH	120	111.9	117.4	107.3	-2.2%	-4.1%
20	4000	2300	-20	75	BCPH	120	114.9	117.3	109.2	-2.3%	-5.0%
21	6000	2300	-20	75	BCPH	120	117.8	116.6	110.9	-2.9%	-5.9%
22	2000	2300	0	75	BCPH	120	115.5	117.0	109.7	-2.5%	-5.0%
23	4000	2300	0	75	BCPH	120	118.6	116.9	111.6	-2.6%	-5.9%
24	6000	2300	0	75	BCPH	120	121.6	116.0	113.1	-3.3%	-6.9%
25	2000	2300	20	75	BCPH	120	118.9	117.3	112.0	-2.3%	-5.8%
26	4000	2300	20	75	BCPH	120	122.0	117.0	113.7	-2.5%	-6.8%
27	6000	2300	20	75	BCPH	120	124.9	116.0	115.2	-3.4%	-7.8%
							Standard Deviation			1.0%	1.4%

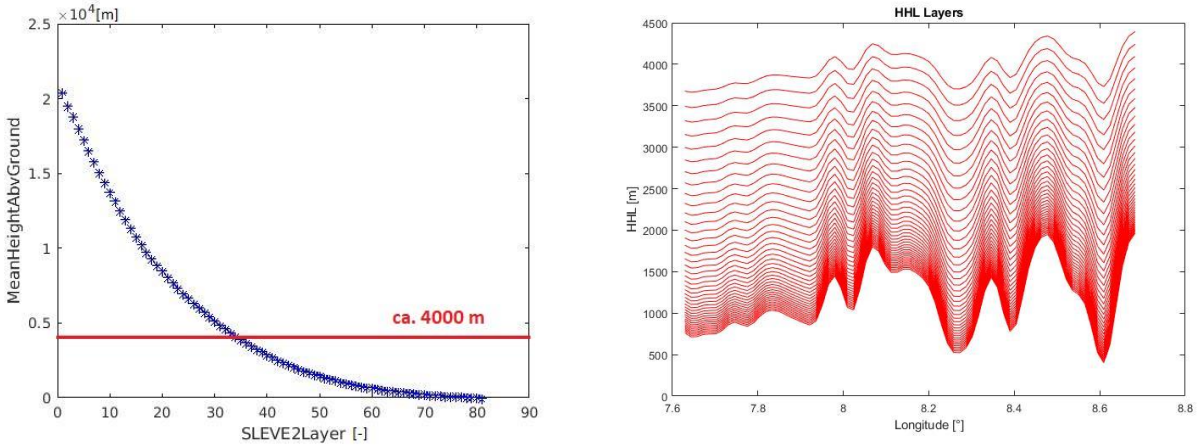

Figure 7 – Selve2 Layers to be evaluated (left), mean height above ground of SELVE2 layers (right)

Prior to correlation calculation, horizontal geometric cartesian layers were interpolated based on the SLEVE2 layers. The interpolation was done every 50 m between the lowest point in the SLEVE2 layers up to 4000 m above sea level. Both meteorological data sets (horizontal layer set and SLEVE2 layer set) were used to try to find a correlation. The slope of the terrain in wind direction was calculated for every SLEVE2 layer as well as every interpolated horizontal layer. Further, the vertical wind provided by COSMOS bases on SELVE2 layers were interpolated on horizontal layers. Totally four datasets were used for correlation calculation. Figure 8 shows the layer with best mean correlation of each dataset. It can be seen that there is no correlation found more than the target value 0.6. Further the Scorer parameter and the Froude number were calculated for all dataset. The maximum correlations of the Score parameter and Froude number are 0.32 and 0.38. Due to the insufficient correlations, Co-Kriging cannot be performed. Therefore, Kriging was used as the downscaling method for vertical wind speeds in this concept study.

Although the Co-kriging of vertical wind fields from in-mean-flow topographic slope proved not to be successful in this phase of the research work, further research needs to be done, as this technique was successful in a number of other studies [36][37][38]. We assume that the variogram should have been generated based on a larger area-averaged topographic fields, as the air must be considered as an inertial medium, reacting mainly to larger mountain ridges. Additionally, wave may propagate non-parallelly to the mountain ridge with altitude, as well as have a horizontal propagation velocity, leading to non-standing gravity waves.

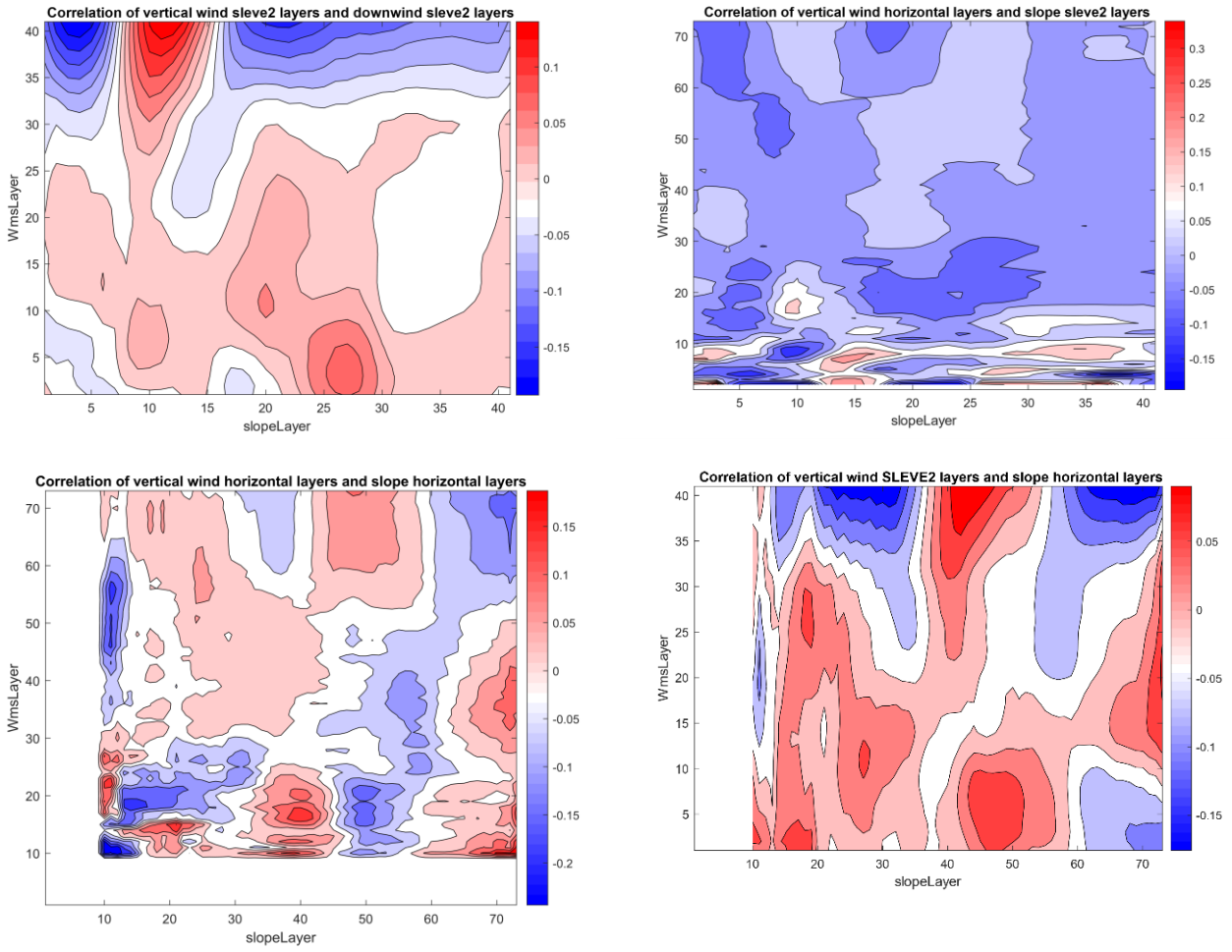

Figure 8 – Correlation of vertical wind and terrain slope

3.2.2 Kriging

Comparison between kriging results and data from weather stations

The Kriging results were compared with the data from weather stations. Table 3 summarizes the locations of the weather stations in the considered mountainous region near Piz Bernina.

Table 3 – Weather stations in the region around Bernina

Weather station	*Altitude ASL*	*WGS84*	*CH1903+*
Lagalb (Diavolezza)	2979 m	46.41° N	142'989 N
		9.97° E	794'610 E
Piz Lagrev	3164 m	46.45° N	146'844 N
		9.72° E	775'267 E
Piz Corvatsch	3315 m	46.42° N	143'739 N
		9.82° E	783'048 E
Passo del Bernina	2260 m	46.41° N	143'020 N
		10.02° E	798'413 E

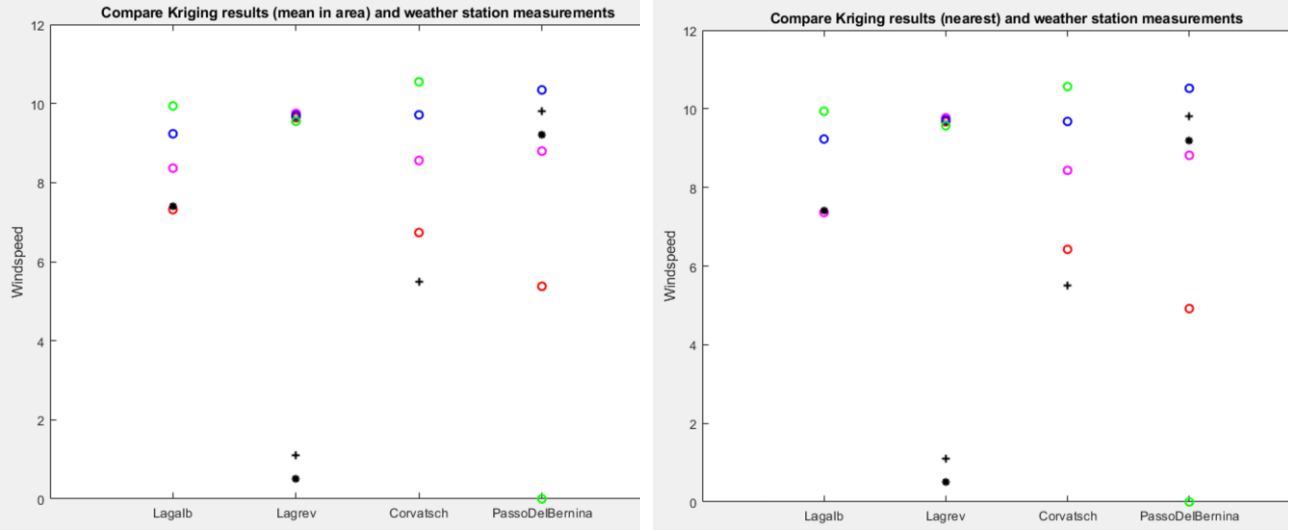

Figure 9 – Comparison of weather station data and windspeed in [m/s] from Kriging of COSMO data (left: mean 1 km^2 around weather station, right: nearest point to weather station)

The Kriging results were compared with the data from weather stations. Table 3 summarizes the

red circle:	Kriging result from COSMO data from the same altitude as the weather station
magenta circle:	Kriging result from COSMO data from 100 m above the weather station.
blue circle:	Kriging result from COSMO data from 200 m above the weather station
green circle	Kriging result from COSMO data from 300 m above the weather station
black plus	mean over 1 hour (except for Corvatsch where it is over 10 min) for the time starting at 13.00 UTC
black asterisk	mean over 1 hour for the time starting at 12.00 UTC

Figure 9 compares the horizontal wind data gathered from weather stations and from COSMO at 13:00 UTC on18th of November 2017. Nearest-neighbouring grid cell data averaged over one km^2 were chosen for the comparison between the two datasets. The comparison of Kriging data with actual wind data measured at the respective day shows that for all weather stations except Lagrev, the measured data lies in the range of values given by the Kriging data 100 to 300 meters above the station. The magnitude of the Kriging data is therefore a reasonable approach to real data. The difference between the both (closest point to the weather station) is not significant. This can be accounted to the way the value of a data point generated by Kriging is related to surrounding values.

Comparison between kriging results and PALM data

PALM simulations were carried out using COSMO data from 09:00 UTC to 15 U The calculation domain locates at 133'915 – 152'347 latitude and 774'572 to 799'148 longitude (in CH 1903+coordinates).

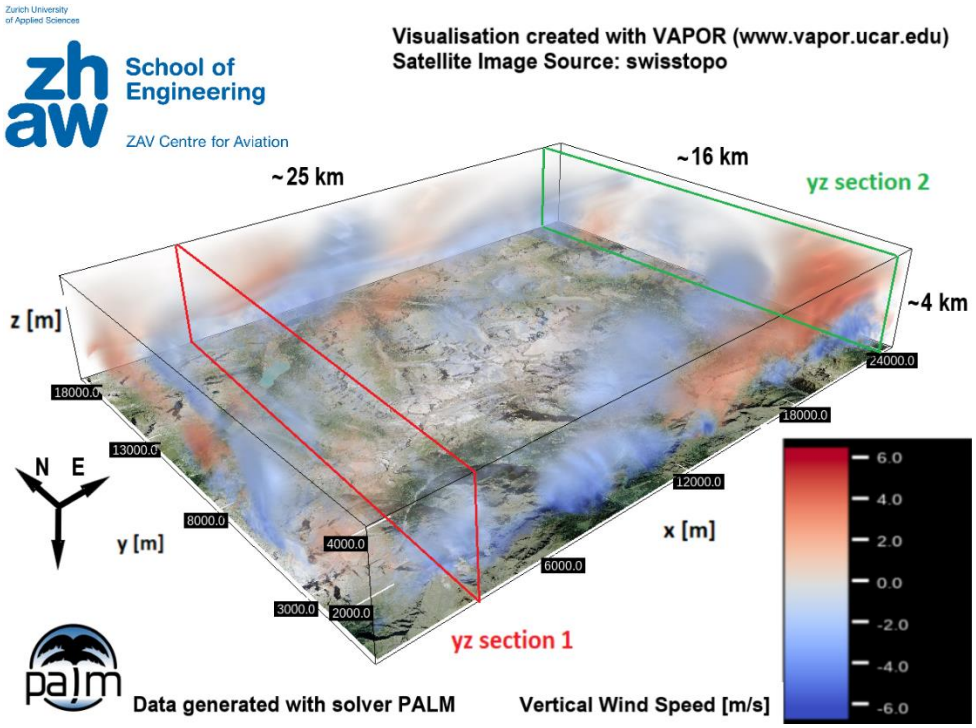

Figure 10 – 3D vertical wind field generated with PALM

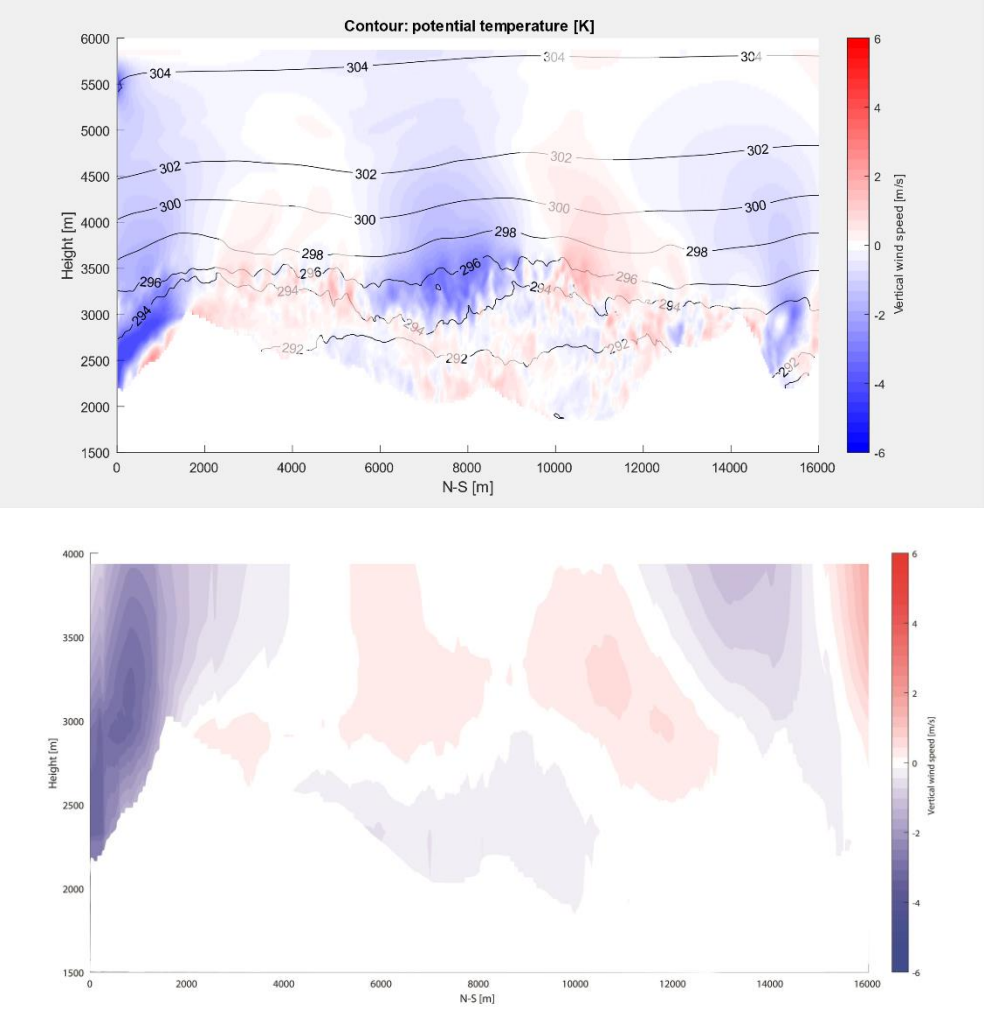

Figure 11 – Y-Z cross section 1 at 777799 E [CH 1903+] of the vertical wind filed from PALM (upper) and kriged COSMO data (low)

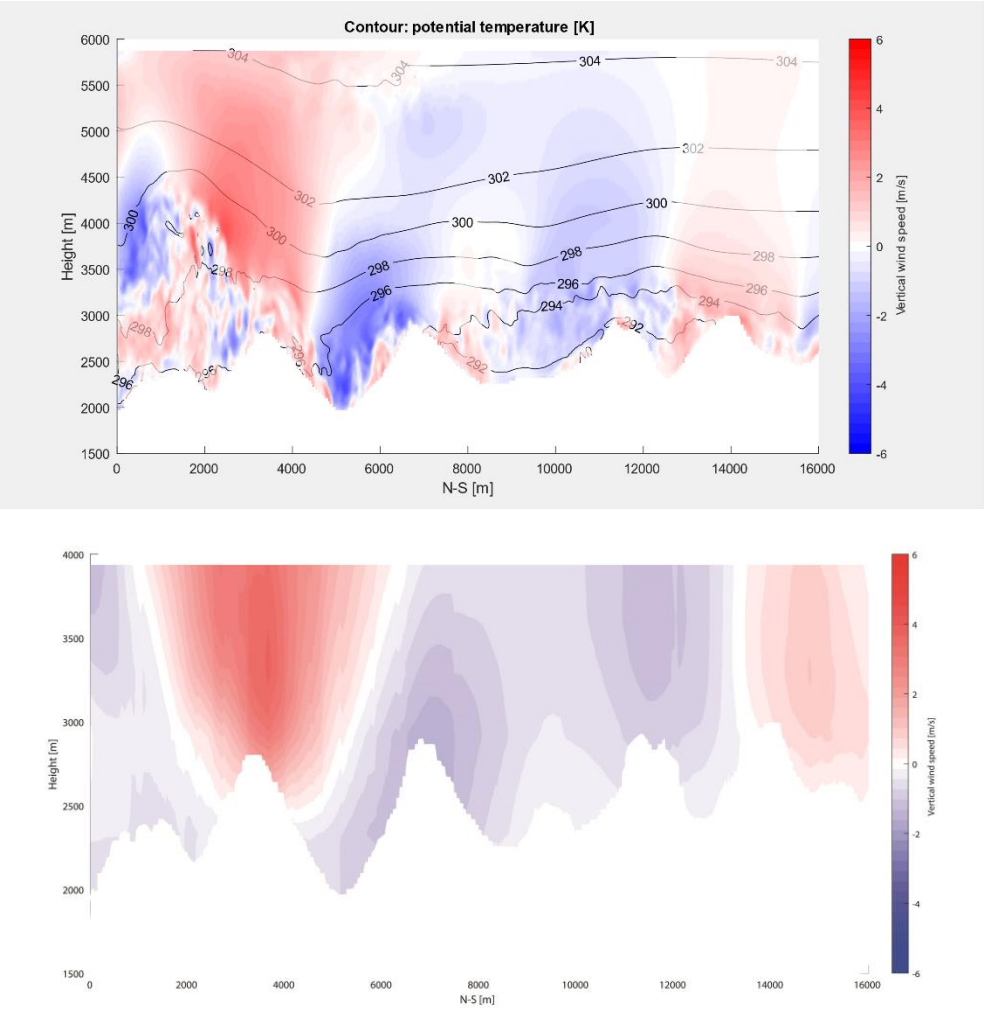

Figure 12 – Y-Z cross section 2 at 798460 E [CH 1903+] of the vertical wind filed from PALM (upper) and kriged COSMO data (low)

Figure 10 shows the 3D PALM results of averaged vertical wind speeds over one hour (18th of November 2017 from 12:30 to 13:30 UTC) on the entire calculation domain. Further, the vertical wind speeds were plotted on two yz-nord-south cross sections and compared with Kriging data (see Figure 11 and Figure 12). The results of PALM and the kriging data show qualitatively comparable patterns, although the two datasets have quantitively significant differences in some orographically complex areas. Those differences can be explained by the difference geometric orientation of the lee-waves, which possible originates from the geographical domain configuration of PALM. In the concept study, the two datasets are considered as acceptable for the demonstration purpose in this phase. As results of this work package, 3D fields generated with PALM were fed into the flight simulator on the one hand, the kriging data were integrated into the EMGA GUI on the other hand.

3.3 Summary of flight simulation test

In the last step of the concept study, a new flight simulation environment based on the results of the previous sections was built in the flight simulator ReDSim. In order to test the first implementation, a series of pilot-in-the-loop simulation tests were conducted. A group of experience were invited to test the implementation in the ReDSim. Every test session was debriefed with an interview with the test pilots. A comprehensive flight test plan was established prior to the test. This section gives a summary of the test campaign.

Technical setup

As previously explained, in order to generate highly resolved wind fields in the ReDSim, the data from PALM simulations were used, focusing on a small mountainous region in Switzerland. PALM was

driven with boundary conditions extracted from the COSMO-1 reanalysis of MeteoSwiss. Besides, the same COSMO-1 data were downscaled using kriging method and integrated in the EMEAG GUI. The EMEGA GUI was used as assistant system which provides pilots with flight performance information and a risk map predicting vertical wind speed. The test scenarios were defined based on the published accidents reports from STSB. The corresponding COSMO data on these test days were provided by MeteoSwiss. As example, Figure 13 shows one of the tested scenarios. In this scenario, the atmospheric disturbance model was fully enabled (Dryden turbulence model and PALM data). A pre-defined flight path is sketched in the figure. The airplane performed a steady climb from Sierra (point D) to the test area Diavolezza (point B and C). In the test area, several level turns were performed before heading back to Samedan airport.

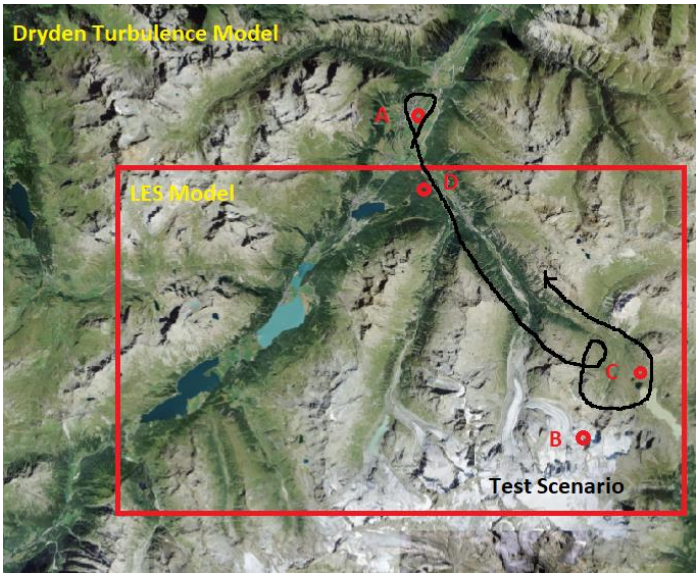

Figure 13 – Pre-defined flight path of a test scenario (A: Samedan airport, B: SwissMetNet station Diavolezza, C: SwissMetNet station Passo del Bernina, D: Sierra)

Human factor assessment

Three experienced pilot tested the functionality of the tool (seven modules of EMEGA GUI) and provided feedback on its user-friendliness using a standardized questionnaire. A brief description is summarized as follows.

The age of the three test pilots is between 36 and 69 (see Table 4). All three pilots are experienced, and they have engineering backgrounds as well. Pilot 1 and pilot 3 are senior lecturers at the ZHAW. Pilot 3 has completed a large number of flight hours in his career.

Due to the small sample size, no statistical analysis was carried out. The results of the assessment of the various modules in EMEGA GUI are shown as bar charts. The evaluation scale comprises 7 levels (1 = not applicable at all; 7 = fully applicable). As example, Figure 14 presents the assessment of the module risk map which displays flight route and provides meteorological information. The detailed assessment of the flight route in the risk map was assessed by all three pilots. The completeness is consistently rated highly. Clarity, comprehensibility and legibility are rated critically by pilot 2, while pilots 1 and 3 rate them as high. In addition to these quantitative assessments, the made detailed suggestions for improving the graphic display (enlarge font and buttons, use thicker lines and stronger colors) and other features of the tool. In response to the open questions, the module excess power for level turn is specifically highlighted (pilot 1), emphasized is the importance of the provided information for flying in the mountains (pilot 3) and in general, pilot 2 finds the idea of the research project good. To the open question about negative aspects, pilot 2 replies that the tool might be too scientific. The pilots need a simpler representation, possibly with less information. Pilot 3 points out that the tool could be too complicated for private pilots, especially if they were additionally absorbed by switching between the modules of the tool during periods of high stress on their flying skills. Considering those feedbacks, some standards, e.g. the concept of ecological primary flight display introduced in [37], needs to be applied for the prototype development in the next phase of the research work.

Table 4 – Characteristics of test pilots

Person	Age	Flight hours	Background
Pilot 1	49	6’750	airline pilot, informatics engineer, senior lecturer in aviation
Pilot 2	36	4’830	airline pilot, mechanical engineer, aerobatics instructor
Pilot 3	69	22’400	former airline pilot, informatics engineer, senior lecturer in aviation

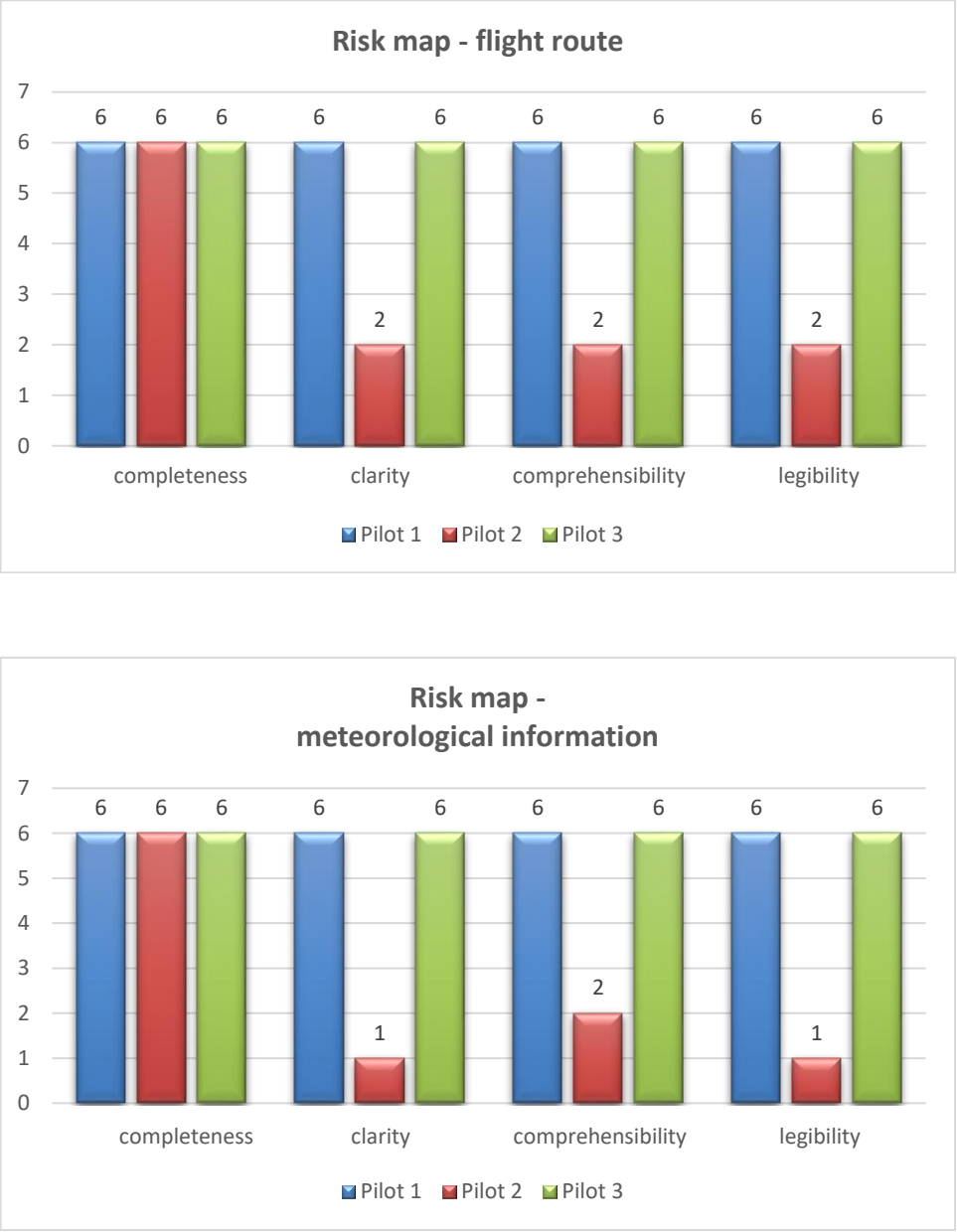

Figure 14 – Bar chart to design the module “Risk map” in EMEGA GUI: flight route (upper) and meteorological information (low)

4. Conclusion and outlook

The ZAV of ZHAW is working on developing an energy management system The goal of the completed concept study is for the remaining energy reserves of the aircraft to be displayed to the pilot as simply and reliably as possible by means of suitable sensors which combine measured-/parameterized influences of meteorological parameters and the modelling of flight performance. As a result, the pilot can perform the necessary flight manoeuvres and adapt them to the situation so that the power envelope of the aircraft is not exceeded.

In the phase I – concept study of the research project, a new fight simulation environment was built to test the first implementation of the energy management system. A series of flight simulation test were successfully conducted with experienced pilot. Further, first feedbacks on user-friendliness of the developed tool were assessed using a standardized questionnaire in the field of human factors. The first version of the tool was generally rated as useful, although further development is required. Therefore, the feasibility of the concept has been proved during this study.

The second phase of the research work aims to develop a prototype system with this new innovative technology that will be installed a test airplane. A series of flight would then be carried out to assess the effectiveness of the system in real world conditions. The phase II project is solution-oriented and closer to the practical realm. The research work would pave the way from fundamental research to practical application. It is composed of the five main work packages: 1) extension of currently developed mathematical models (flight performance and meteorology), 2) flight simulations tests with upgraded EMEGA system, 3) system integration including design and implementation of primary flight display, 4) flight testing with a large group of pilots (GA pilots as well), 5) further human factors assessment und 6) dissemination and exploitation – prepare the path to the market.

5. Contact Author Email Address

Mailto: xinying.liu@zhaw.ch

6. Copyright Statement

References

[1] Inokuchi H, Tanaka H and Ando T. Development of an Onboard Doppler Lidar. *26th International Congress of the Aeronautical Sciences,* Anchorage, Alaska, USA, 2008.

[2] Matayoshi N, Iijima T, Uemura T, Yoshikawa E, Entzinger J-O, Uemura T, Akiyama Tand Inokuchi H. Development and Flight Demonstration of a New Lidar-Based Onboard Turbulence Information System. *31st International Congress of the Aeronautical Sciences,* Belo Horizonte, Brazil, 2018.

[3] Inokuchi H, Akiyama T and Sasaki K. Flight Demonstration of a Long Range Onboard Doppler Lidar. *31st International Congress of the Aeronautical Sciences,* Belo Horizonte, Brazil, 2018.

[4] Iijima T, Uemura T, Matayoshi N, Entzinger J-O, Matsumoto J, Ueda S and Yoshikawa E. Development and Evaluation of a New Airspeed Information System utilizing Airborne Doppler Lidar for Flight Safety. *IEEE/AIAA 36th Digital Avionics Systems Conference (DASC),* St. Petersburg, Florida, USA, 2017.

[5] Siepenkötter N, Moormann D. Precision Landing Based on Atmospheric Disturbance Monitoring and Model Predictive Control. 30th *International Congress of the Aeronautical Sciences,* Daejeon, Korea, 2016.

[6] Vrancken P, Wirth M, Ehret G, Barny H, Rondeau P and Veerman H. Airborne forward-pointing UV Rayleigh lidar for remote clear air turbulence detection: system design and performance. *Applied Optics*, Vol. 55, Issue 32, pp 9314-9328,2016.

[7] European Aviation Safety Agency – Safe Analysis & Research Department. Annual Safety Review 2014, pp 42-47, 1954.

[8] U.S. Department of Defense. MIL-F-8785: Military Specification – Flying Qualities of Piloted Airplanes, technical report, 1954.

[9] Spillmann. Flight Testing of a General Aviation Aircraft and Aerodynamic Model Estimation, master thesis, ZHAW Switzerland 2019.

[10] Lycoming. Operator's Manual Lycoming O-320 Series, 3rd Edition, Part No. 60297-30, 2006.

[11] Piper Aircraft Corporation. Pilot's Operating Handbook Warrior II PA-28-161, 1982

[12] Suter S, Konzelmann T, Mühlhäuser C, Bergert M and Heimo A. SwissMetNet- The New Automatic Meteorological Network of Switzerland: Transition from Old to New Network, Data Management and First results. *6th European Conference on Applied Climatology*, Ljublijana, Slovenia,2006.

[13] Myers D.E. Pseudo-Cross Variograms, Positive-Definiteness, and Cokriging. *Mathematical Geology*, Vol. 23, No. 6, pp 805-816, 1991.

[14] Clark I, Basinger K.L and Harper W.V. Muck – a novel approach to co-kriging. *Proceedings of the Conference on Geostatistical, Sensitivity, and Uncertainty: Methods for Ground-Water Flow and Radionuclide Transport Modeling: Batelle Press*, p.473 -494, 1989

[15] Raasch S, Schröter M. PALM – a large-eddy simulation model performing on massively parallel computers. *Meteorologisch Zeitschrift*, Vol. 10, No. 5, pp 363-372, 1999.

[16] Maronga B, Gryschka M, Heinze R, Hoffmann F, Kanani-Sühring F, Keck M, Ketelsen K, Letztel M.O, Sühring M and Raasch S. The Parallelized Large-Eddy Simulation Model (PALM) version 4.0 for atmospheric and oceanic flows: model formulation, recent developments, and future perspectives. *Geoscientific Model Development*, Vol. 8, No. 8, pp 2515-2551, 2015.

[17] Maronga B, Banzhaf S, Burmeister C, Esch T, Forkel R, Fröhlich D, Fuka V, Gehrke K, Geletič J, Giersch S, Gronemeier T, Gross G, Heldens W, Hellsten A, Hoffmann F, Inagaki A, Kadasch E, Kanai-Sühring F, Ketelsen K, Basit Ali Khan, Knigge C, Knoop H, Krč P, Kurppa Mona, Maamari H, Matzarakis A, Mauder M, Pallasch M, Pavlik D, Pfafferott J, Resler J, Rossmann S, Russo E, Salim M, Schrempf M, Schwenkel J, Seckmeyer G, Schubert S, Sühring M, Robert von Tils, Vollmer L, Ward S, Witha B, Wurps H, Zeidler J, and Raasch S. Overview of the PALM model system 6.0. *Geoscientific Model Development*, Vol. 13, No. 3, pp 1335-1372, 2020.

[18] Fluck S, Anet J. Large Eddy Simulation des Piz Segnas-Gebietes, technical report, ZHAW Switzerland, 2019.

[19] Arakawa A and Lamb V. Computational Design of the Basic Dynamics Processes of the UCLA General Circulation Model. *Methods in Computational Physics: Advances in Research and Applications,* Vol. 17, pp 173-265, 1977.

[20] Patrinos A and Kistler A. A numerical study of the Chicago lake breeze. Boundary-Layer Meteorology, Vol. 12, pp 93-123, 1977.

[21]Dearorff J. Stratocumulus-capped mixed layers derived from a three-dimensional. *Boundary-Layer Meteorology*, Vol. 18, pp 495-527, 1980.

[22]Moeng C and Wyngaard J. Spectral Analysis of Large-Eddy Simulations of the Convective Boundary Layer. *Boundary-Layer Meteorology*, Vol. 45, No. 23, pp 3573-3587, 1988.

[23]Saiki E, Moeng C and Sullivan P. Large-Eddy Simulation of the Stably Stratified Planetary Boundary Layer. *Boundary-Layer Meteorology*, Vol. 95, pp 1-30, 2000.

[24]Heinz S, Mokhtarpoor R. Dynamic large eddy simulation: Stability via realizability. *Physics of Fluids*, Vol. 29, No. 10, 2017.

[25]Holt T, Raman S. A review and comparative evaluation of multilevel boundary layer parametrizations for first-oder and turbulent kinetic energy closure schemes. *Review of Geophysics*, Vol. 26, No. 4, 761-780, 1988.

[26]Mellor G, Yamada T. A Hierarchy of Turbulence Closure Models for Planetary Boundary Layers. *Journal of the Atmospheric Sciences*, Vol. 31, No. 7, pp 1791-1806, 1974.

[27]Mellor G, Yamada T. Development of a turbulence closure model for geophysical fluid problems. *Review of Geophysics*, Vol. 20, No. 4, pp 851-875, 1982.

[28]Wicker L, Skamarock W. Time-Splitting Methods for Elastic Models using Forward Time Schemes. *Monthly Weather Review*, Vol. 130, No. 8, pp 2088-2097, 2002.

[29]Williamson J. Low-storage Runge-Kutta schemes. *Journal of Computational Physics,* Vol. 35, No. 1, pp 48-56, 1980.

[30]Lund T, Wu X and Squires K. Generation of turbulent inflow data for spatially-developing boundary layer simulations. *Journal of Computational Physics*, Vol. 140, No. 2, pp 233-258, 1998.

[31]Kataoka H, Mizuno M. Numerical flow computation around aeroelastic 3D square cylinder using inflow turbulence. *Wind and Structures*, Vol. 5, No. 2, pp 379-392, 2002.

[32]Liu X, Manfriani L and Fu Y. Doctoral Dissertation Literature Review: Synthesis of Meteorological and Orographic Influences on the Safe Energy Envelope of an Airplane. Beihang University China, ZHAW Switzerland, 2020.

[33]Ferrari F. Flight Testing of A General Aviation Aircraft and Aerodynamic Model Estimation, master thesis, ZHAW Switzerland, 2019.

[34]Um M, Kim Y. E. Estimating potential wind energy from sparsely located stations in a mountainous coastal region. *Meteorological Applications*, Vol. 24, No. 2, pp 279-289, 2017.

[35]Joyner T, Friedland C, Rohli R, Treviño A, Massarra C and Paulus G. Cross-correlation modeling of European windstorms: A cokriging approach for optimizing surface wind estimates. *Spatial Statistics*, Vol. 13, pp 62-75, 2015.

[36]Parker S, Taylor M and Luo W. A comparison of spatial interpolation methods to estimate continuous wind speed surfaces using irregularly distributed data from England and Wales. *International Journal of Climatology*, Vol. 28, No. 7, pp 947-959, 2007.

[37]Lambregts T, radeaker R and Theunissen E. A new ecological primary flight display. *IEEE/AIAA 27th Digital Avionics Systems Conference (DASC),* St. Paul, Minnesota, USA, 2008.